Nanoscale

Accepted Manuscript

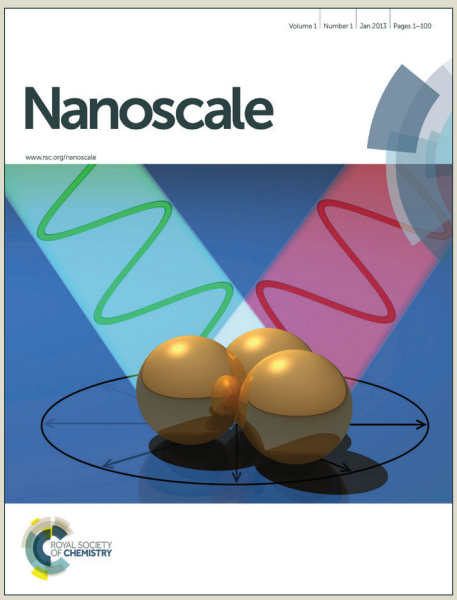

ROYAL SOCIETY OF CHEMISTRY

www.rsc.org/nanoscale

Cite this: DOI: 10.1039/c0xx00000x

www.rsc.org/xxxxxx

Communication

Morphological control and evolution of octahedral and truncated trisoctahedral Pt-Au alloy nanocrystals under microwave irradiation

Lei Dai,[a] Yanxi Zhao,[a] Quan Chi,[a] Hanfan Liu,[a,b] Jinlin Li,[a] and Tao Huang*[a]

Received (in XXX, XXX) Xth XXXXXXXXX 20XX, Accepted Xth XXXXXXXXX 20XX

DOI: 10.1039/b000000x

Uniform and well-defined truncated trisoctahedral and octahedral Pt-Au alloy nanocrystals were fabricated by co-reducing H_2PtCl_6/$HAuCl_4$ with tetraethylene glycol (TEG) under microwave irradiation for only 140 s. Iodide ions were critical to the morphological control and evolution of Pt-Au alloy nanostructures. The as-prepared Pt-Au alloy nanocrystals exhibited efficient electrocatalytic activities.

Bimetallic alloy or core-shell nanostructures with uniform sizes and well-defined morphologies have been paid much attention for decades owing to their unique properties and potential applications in catalysis, optics, and electronics.[1] Especially, their properties, which are strongly dependent upon their sizes, shapes, compositions and surface structures, may be superior to those of the corresponding monometallic nanoparticles because of their tunable elemental compositions as well as the synergistic effects between bimetal components.[2] Up to now, a lot of efforts have been devoted to the shape-controlled synthesis of bimetallic nanoparticles, and many bimetallic nanocrystals with core-shell or alloy structures have been obtained. Generally, a two-step seed-mediated method[3] has been widely used to generate bimetallic core-shell nanocrystals with special geometries though a few one-step strategies were also used,[4] while galvanic replacement,[5] Kirkendall effect[6] or/and co-reduction[2a,4] as well as their simultaneous or sequential action[5g] have usually been employed to prepare shaped bimetallic alloy nanoparticles. However, compared with the preparation of bimetallic core-shell nanostructures, shape-controlled synthesis of bimetallic alloy nanocrystals is more difficult due to complicated reduction kinetics of two metal precursors.[7] Thus, development of a facile and simple method for synthesis of bimetallic alloy nanocrystals with special morphologies remains a great challenge.

As the most chemically stable noble metals and promising nanomaterials in technological applications, nanoscale Pt and Au have been widely researched. In particular, it has been reported that bimetallic Pt-Au alloy or core-shell nanostructures exhibited more unusual catalytic properties than pure Pt and pure Au. For instance, Pt-Au alloy demonstrated outstanding electrocatalytic performance for oxygen reduction,[8] methanol oxidation in fuel cells because the Au composition suppressed the adsorption of poisoning species such as CO.[2a,9] So far, bimetallic Pt-Au nanoparticles with various morphologies such as core-shell concave nanocubes,[10] nanowires,[11] nanorods,[12] cage-bell,[13] clover,[14] as well as alloy nanocubes,[4d] icosahedra,[15] nanodendrites[16] and mesoporous nanocrystals[2a] have been prepared. Generally, however, it is very difficult for the formation of a homogenous bimetallic Pt-Au alloy state due to the different reduction kinetics of Pt(IV) and Au(III) ions, as well as complex reaction environment in solution.[17] The phase segregation was often reported.[18] Therefore, the creation of bimetallic Pt-Au alloy nanoparticles is worthy of exploring.

Herein, microwave irradiation was employed in the shape-controlled synthesis of bimetallic Pt-Au alloy nanocrystals, and unique single-crystalline truncated trisoctahedral Pt-Au alloy nanostructures as well as octahedral Pt-Au alloy nanocrystals were obtained in a high yield by one-step method with no assistance of pre-synthesized seed or template under microwave irradiation in an extremely short time. The presence of iodide ions was critical to the formation of Pt-Au alloy nanocrystals by adjusting the reduction kinetics of Pt and Au precursors. Iodide ions, microwave penetration as well as co-reduction of Pt and Au precursors gave a fine control over the nucleation and growth kinetics, resulting in the formation of Pt-Au alloy nanostructures with well-defined shapes. The electrocatalytic properties of the as-prepared Pt-Au alloy nanocrystals were also investigated.

In a typical synthesis, together with the use of tetraethylene glycol (TEG) as both a solvent and a reducing agent, a mixed solution of H_2PtCl_6/$HAuCl_4$ with a molar ratio of 1/1 in TEG was reduced simultaneously under microwave irradiation for 140 s in the presence of polyvinylpyrrolidone (PVP) and potassium iodide (KI) (see **ESI** for details). The representative transmission electron microscopy (TEM) images and scanning electron microscopy (SEM) images of the as-prepared samples are presented in **Fig. 1**a and b, respectively, as well as **Fig. S1, ESI** †. As can be seen, all the particles showed trisoctahedral shapes with an average size of about 200 nm. Particularly, the trisoctahedral nanoparticles illustrated truncated feature, as shown in **Fig. 1**c_1 which displayed one pod of a single particle. The geometrical model of a truncated trisoctahedraon is shown in **Fig. S2, ESI**†. **Fig. 1**c_2, c_3 and c_4 presented individual Pt-Au particle along <111>, <110>, and <100> directions, respectively, as described in the corresponding inset models. The high-angle annular dark-field scanning transmission electron microscopy (HAADF-STEM) image with the same luminance indicates the alloy structure of the as-prepared Pt-Au nanocrystals rather than a core-shell structure (**Fig. 1**d).[2a, 4d, 18b,c] The truncated feature can also be visible from HAADT-STEM images (**Fig. S**3, **ESI**†). The HRTEM image (**Fig. 1**e) and the corresponding fast

Fourier transform (FFT) pattern (**Fig. 1**f) demonstrated well-resolved and continuous crystal lattice clearly, revealing a single crystalline structure and good crystallinity for an individual truncated trisoctahedral Pt-Au nanocrystal. The single-crystal feature was ascribed to their same face-centered cubic (*fcc*) structures.

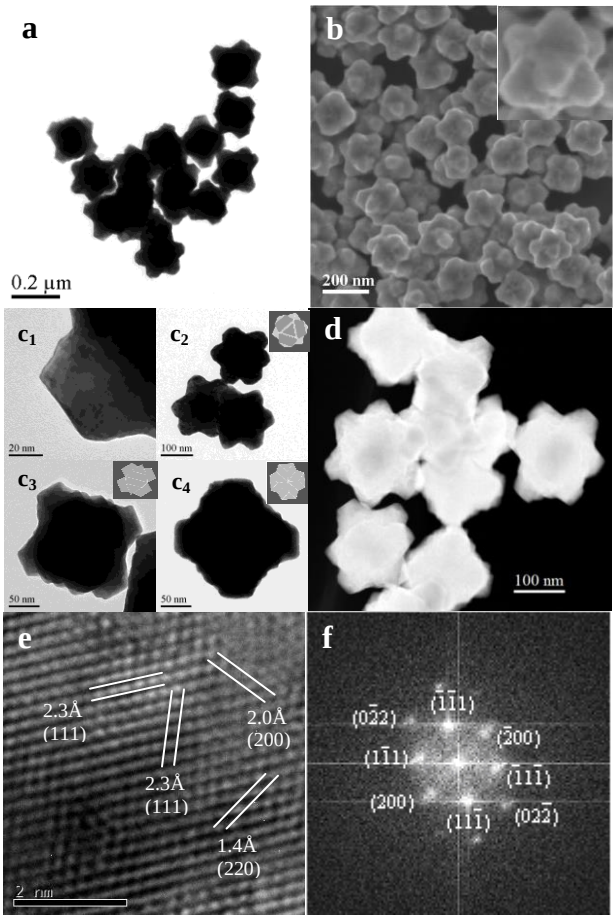

Fig. 1 (a) Typical TEM and (b) SEM of the truncated trisoctahedral Pt-Au alloy nanocrystals; (c) TEM images of an individual Pt-Au alloy truncated trisoctahedron (c_1: one pod; c_2-c_4: projections along <111>, <110> and <100> directions; The insets are the corresponding structure models, respectively); (d) HAADT-STEM image; (e) HRTEM image and f) the corresponding FFT pattern.

The energy dispersive X-ray spectroscopy (EDX) elemental mapping further revealed that the as-prepared truncated trisoctahedral structure was made of Pt-Au alloy without phase segregation, as shown in **Fig. 2**a_1 (HAADF-STEM), a_2 (green, Pt), a_3 (red, Au) and a_4 (overlap, Pt-Au). The elemental composition analyses exhibited the presence of 54 atomic%Pt and 46 atomic% Au (**Fig. 2**b). The Pt-Au alloy state and the elemental distributions were also confirmed by EDX line scanning profiles across a single particle along the frontage diagonal (**Fig. 2**c) and the central waistline (**Fig. 2**d), showing an identical distribution of both Pt and Au in different directions with a slightly higher abundance of Pt.

The dependence of the morphological evolution upon the reaction time was investigated. When irradiating for 100 s, particles with an average size of about 100 nm were produced and the trisoctahedral feature was unobvious (**Fig. S4**a, **ESI**†). When the irradiation time was increased to 120 s, the trisoctahedral structures with a distinct truncated feature and a bigger size were generated (**Fig. S4**b, **ESI**†). However, with increasing the irradiation time to 160 or 180 s, no significant changes in the structure and size were observed (**Fig. S4**c and d, **ESI**†). Moreover, the XRD patterns for the products obtained at 100, 120, 140, and 160 s show that the as-prepared Pt-Au alloy truncated trisoctahedra can be identified as *fcc* structures and all the diffraction peaks appeared at 2θ values between those of pure Au (JCPDS No. 04-0784) and pure Pt (JCPDS No. 04-0802) as single peaks (**Fig. S5**, **ESI**†). Especially, the 2θ values remained unchanged for all the samples obtained from 120 to 160 s (**Table S1**, **ESI**†). These results proved that not only the as-prepared Pt-Au nanoparticles were indeed an alloy rather than a mixture of monometals or core-shell structure,[2a, 4d, 18b,c] but also the formation of Pt-Au alloy nanostructures should be attributed to co-reduction of the metal precursors.

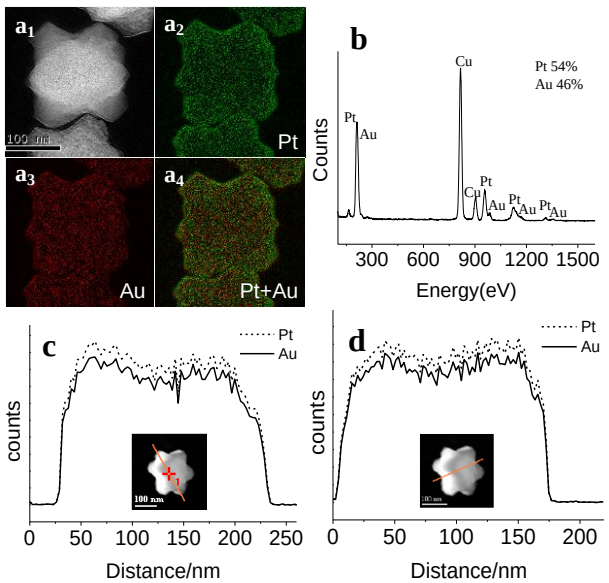

Fig. 2 (a) HAADT-STEM image (a1) together with EDX mapping images of the selected Pt-Au alloy truncated trisoctahedron (a2: green=Pt; a3: red=Au; a4: overlap of Pt and Au); (b) EDX spectrum of the Pt-Au alloy truncated trisoctahedra; (c) and (d) Line-scanning profiles across a single particle along the frontage diagonal and the central waistline, respectively

Dramatically, under the same other conditions and the same total concentration of metal precursors, Pt-Au octahedral nanostructures with an average size of about 130 nm were obtained in a high yield when the molar ratio of Pt(IV)/Au(III) was tuned to 1/3, as the TEM and SEM images presented in **Fig. 3**a and b, as well as **Fig. S6** (**ESI**†), respectively. **Fig 3**c_1 and c_2 show the TEM images of individual Pt-Au octahedral nanoparticles oriented along <100> and <110> directions, respectively, while both of **Fig. 3**c_3 and c_4 show <111> orientations.

It is especially noteworthy that XRD patterns of Pt-Au octahedral nanocrystals demonstrated a significantly different absorption feature compared with that of Pt-Au alloy truncated trisoctahedra. As shown in **Fig. 3**d, only two peaks derived from

Pt-Au octahedral nanocrystals can be observed obviously. An extremely strong sharp peak at 38.25° and a much weak peak at 81.88° can be indexed to (111) and (222) facets of *fcc* structure, while other peaks corresponding to (200), (220) and (311) facets are too weak to distinguish. These observations indicated that the preferential orientation of Pt-Au octahedral structure was {111} surfaces in the case of 1/3 of Pt(IV)/Au(III) molar ratio. This was consistent with the surface structure of Pt or Au octahedron enclosed by {111} planes.[19] Moreover, each of the two peaks appeared between that of pure Au and pure Pt as a single peak, and the peaks were much closer to that of Au compared to Pt, revealing a single-phase alloy state with more abundant Au than Pt for the as-prepared Pt-Au octahedra. The HRTEM (**Fig. 3**e) image and the corresponding FFT pattern (**Fig. 3**f) further confirmed their single crystalline structure.

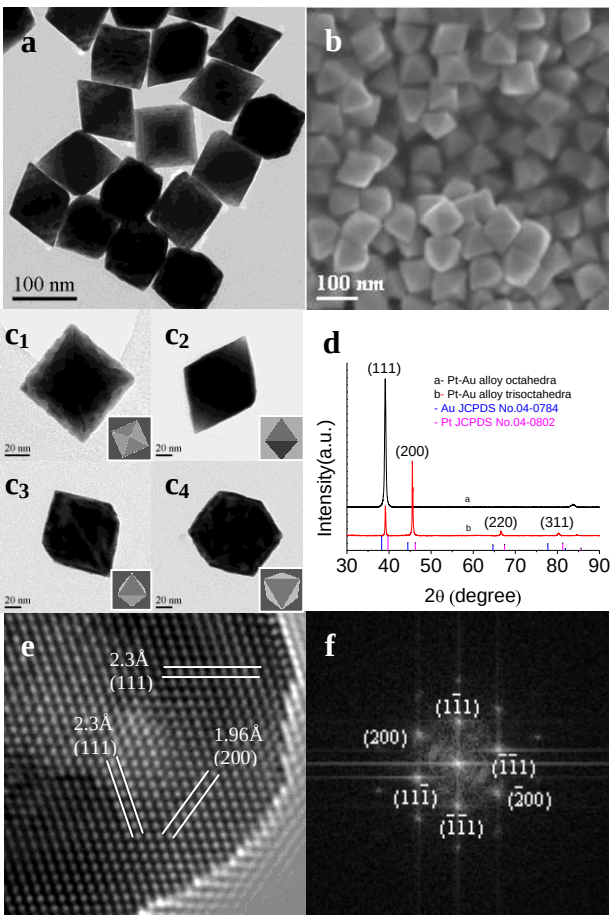

Fig. 3 (a) Typical TEM and (b) SEM of the as-prepared Pt-Au alloy octahedra; (c) TEM images of an individual Pt-Au alloy octahedron projected along <100>, <110> and <111> directions. The insets are the corresponding structure models, respectively; (d) XRD pattern of the octahedral and truncated trisoctahedral Pt-Au alloy nanocrystals as well as the standard XRD patterns of pure Au and pure Pt; (e) HRTEM image and (f) the corresponding FFT pattern..

The EDX elemental mapping images further revealed that the as-prepared Pt-Au octahedron was made of an alloy with homogenous distribution of both Au and Pt throughout (**Fig. 4**a). The elemental composition analyses showed that the atomic percentage of Pt and Au was 32 atomic% and 68 atomic%, respectively (**Fig. 4**b). The elemental compositions and alloy structure were also supported by EDX line scanning profiles through the vertices and middle planes of a single Pt-Au octahedron as shown in **Fig. 4**c and d, respectively. The HAADF-STEM images with the same luminance further confirmed their alloy structures rather than core-shell structures (**Fig. S7**, **ESI†**)

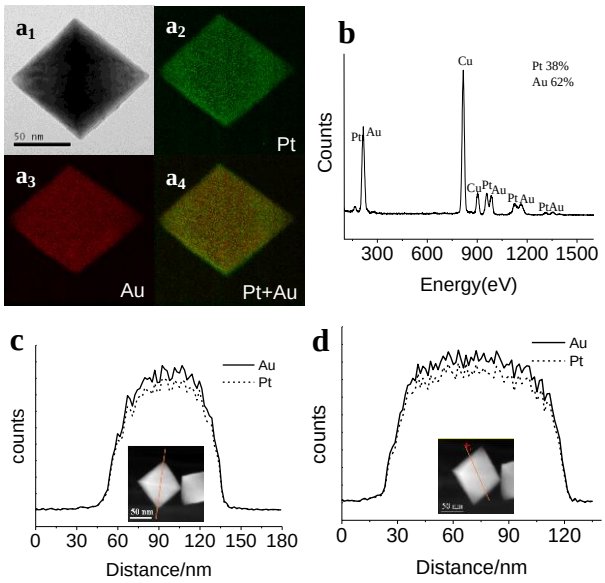

Fig. 4 (a) HAADT-STEM image of an individual Pt-Au alloy octahedron (a1) together with the corresponding EDX mapping images (a2: green=Pt; a3: red=Au; a4: overlap of Pt and Au); (b) EDX spectrum of the Pt-Au alloy octahedra; (c) and (d) Line-scanning profiles through the vertices and middle planes of a single Pt-Au octahedron, respectively.

Furthermore, the XPS spectra of the Pt^0 4f regions and Au^0 regions for both truncated trisoctahedral Pt-Au alloy (the binding energies of $Pt4f_{7/2}$ and $Pt4f_{5/2}$ at 71.33 and 74.70 eV, while $Au4f_{7/2}$ and $Au4f_{5/2}$ at 84.10 and 87.80 eV, respectively) and octahedral Pt-Au alloy nanocrystals (the binding energies of $Pt4f_{7/2}$ and $Pt4f_{5/2}$ at 71.00 and 74.40 eV, while $Au4f_{7/2}$ and $Au4f_{5/2}$ at 83.90 and 87.60 eV, respectively) were shown in **Fig. 5**. The binding energies were close to the standard values (70.80 and 74.15 eV for $Pt4f_{7/2}$ and $Pt4f_{5/2}$, 83.80 and 87.45 eV for $Au4f_{7/2}$ and $Au4f_{5/2}$),[20] indicating Pt^0 and Au^0 with zero oxidation states. It was noteworthy that the binding energies in the Pt regions were negatively shifted with increasing Au content, suggesting that Pt and Au were atomically mixed with no phase separation.[2a,4d]

Interestingly, under the same other conditions, uniform truncated octapodal nanocrystals were generated when the molar ratio of Pt(IV)/Au(III) was changed to 3/1, as shown in **Fig. S8, ESI†**. In absence of Au(III) ions, uniform Pt octapods would be obtained with using single H_2PtCl_6 precursor, as shown in the previous report.[21] Notably, however, under the same conditions, Au(III) ions alone cannot be reduced by TEG in absence of Pt(IV) ions. These results implied that Pt(IV) species were essential for not only the formation of Pt-Au alloy octahedra as well as the morphology evolution with the change of Pt(IV)/Au(III) molar ratio, but also the reduction of Au(III) precursor. Accordingly, the presence of Pt precursor might affect the growth behaviour of Pt-Au bimetallic alloy by interacting with Au(III) precursor or other molecules in the reaction system.

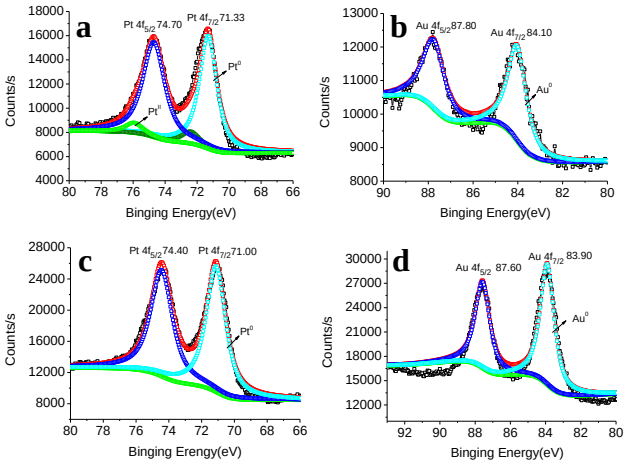

Fig. 5 XPS spectra. (a) Pt 4f and (b) Au4f regions of the as-prepared truncated trisoctahedral Pt-Au alloy nanocrystals; (c) Pt 4f and and (d) Au 4f regions of the as-prepared octahedral Pt-Au alloy nanocrystals.

It was found that the use of KI was critical to the control of the morphologies of Pt-Au alloy nanocrystals and the reduction kinetics. In the absence of KI, only irregular small nanoparticles were produced (**Fig. S9**a, **ESI†**). With addition of 50 mg of KI, Pt-Au nanocrystals with obscure trisoctahedral feature have initially taken shapes (**Fig. S9**b, **ESI†**). In contrast, no obvious change was observed for the Pt-Au alloy truncated trisoctahedra when 200 mg of KI (**Fig. S9**d, **ESI†**) was used compared with the optimum amount (100 mg) of KI. Under the same conditions, an equal amount of KCl or KBr was used instead of KI according to the standard procedure, no trisoctahedral nanostructure but irregular tetrahedral or amorphous particles was obtained (**Fig. S10**, **ESI†**). In addition, it was also found that PVP was important but not essential for the formation of Pt-Au alloy truncated trisoctahedra. In the absence of PVP, Pt-Au alloy truncated trisoctahedra can also be produced though with non-uniform size and a little aggregation (**Fig. S11**, **ESI†**), indicating that PVP served mainly as a protecting and a dispersing agent for the products. Similar results were also observed for the synthesis of Pt-Au alloy octahedra. These results suggest that the formation of either truncated trisoctahedral or octahedral Pt-Au alloy nanocrystals should be attributed to the existence of I^- ions. The I^- ions complexation to metallic ions affected the reducing kinetics. Normally, Au(III) ions should be reduced before Pt(IV) ions because the standard reduction potential ($E°$) for $AuCl_4^-$/Au (+1.000 V *vs*. SHE) is much higher than that of $PtCl_6^{2-}$/Pt (+0.760 V *vs*. SHE). When I^- ions were introduced into the reaction system with TEG solution of H_2PtCl_6/$HAuCl_4$ mixture, more stably coordinated anions $[PtI_6]^{2-}$ and $[AuI_4]^-$ became the dominant species, which would be favourable for the morphological growth of Pt-Au alloy due to lower reduction potentials and slower reducing rates. UV-vis absorption measurements confirmed the transformation of the coordinated anions in the presence of I^- ions. Red shifts occurred for the absorption bands of both $PtCl_6^{2-}$ and $AuCl_4^-$ solution alone, accompanying with changes in color of solution (**Fig. S12**, **ESI†**).

Moreover, in the presence of KI, the reductive peak potential of Au(III) species (+0.240 V *vs*. SCE) became lower than that of Pt(IV) species (+0.325 V *vs*. SCE) (**Fig. S13**, **ESI†**). This observation means that Pt(IV) species would be preferentially reduced prior to Au(III) species. In addition, the potential of Au(III) species became close to that of Pt(IV) species, so that Au(III) ions would also be reduced rapidly in the presence of Pt(IV) ions. Due to I^- ions coordination, the minor difference between the reduction potentials of Au(III) and Pt(IV) species was favorable for their co-reduction, and then Pt-Au alloy nanocrystals grew uniformly from the initial Pt nuclei followed by subsequent or simultaneous co-deposition of Pt and Au atoms. Meanwhile, microwave irradiation changed the growth kinetics by its specific nonthermal effect because microwave irradiation directly activates most molecules and energy transfer occurs in less than a nanosecond (10^{-9} s),[22] promoting the reaction to occur immediately and finish in a rather short time. Thus, microwave irradiation facilitated the co-reduction of Pt(IV) and Au(III) species, thereby making possible the formation of a perfect Pt-Au alloy.

On the other hand, the selective adsorption of I^- ions on some specific facets of Pt and Au guided preferential deposition of Pt and Au atoms derived from co-reduction with the reaction proceeding. I^- ions preferentially adsorbed on Pt {100} facets,[5ab, 23] so that Pt atoms were selectively deposited onto {111} facets, resulting in preferential growth along <111> directions. While the growth of Au {111} facets were inhibited due to the preferential adsorption of I^- ions on Au {111} facets,[24] so that Au atoms were selectively deposited onto {100} facets, leading to preferential growth along <100> directions. Therefore, based on the coordination and selective adsorption of I^- ions, comparable growth along both <111> and <100> directions resulted in the formation of truncated Pt-Au alloy trisoctahedra in the case with an equal amount of Pt and Au precursors. Under the same conditions, Pt-Au alloy octahedra would be generated with a higher amount of Au precursor due to a dominant growth along <100> directions, while Pt-Au truncated octapods would be produced with more Pt precursor due to a dominant growth along <111> directions. Thus, the morphological evolution of Pt-Au alloy nanocrystals with the increase of Au content can be described as follows: Pt octapods → Pt-Au truncated octapods → Pt-Au alloy truncated trisoctahedra → Pt-Au alloy octahedra (**Fig. S14**, **ESI†**).

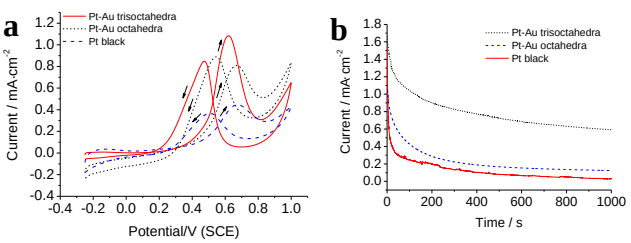

Fig. 6 (a) CV curves for electro-oxidation of methanol by the as-prepared Pt-Au alloy trisoctahedra, Pt-Au alloy octahedra and Pt black, respectively. The methanol oxidation was recorded in 0.1 M $HClO_4$ + 0.1 M CH_3OH solution at a scan rate of 50 mV·s^{-1} between -0.25 and 1.0 V; (b) CA curves for the various catalysts in 0.1 M $HClO_4$ + 0.1 M CH_3OH at 0.62 V *vs* SCE.

The catalytic performances of the as-prepared Pt-Au alloy truncated trisoctahedra and Pt-Au alloy octahedra were investigated by electrocatalytic oxidation of methanol.

Commercial Pt black was used as a reference for comparison. **Fig. 6**a shows the cyclic voltammetry (CV) curves for the electro-oxidation of methanol with different catalysts. The currents were normalized to the electrochemically active surface area (ECSA) of each catalyst, which was calculated by measurement of the Coulombic charge for hydrogen under potential desorption in the CVs of catalysts in 0.1 M $HClO_4$ (**Table S2** and **Fig. S15**, **ESI†**). The peak current densities were measured to be 1.08 and 0.80 $mA{\cdot}cm^{-2}$ on Pt-Au alloy truncated trisoctahedra and Pt-Au alloy octahedra at 0.62 and 0.67 V in 0.1 M $HClO_4$, respectively, demonstrating 2.4 and 1.8 times greater than that of Pt black on which it was 0.45 $mA{\cdot}cm^{-2}$ at 0.67 V. Obviously, though the ECSA of either Pt-Au alloy truncated trisoctahedra or Pt-Au alloy octahedra was smaller than that of Pt black which showed a mean size of about 4.5 nm (**Fig. S16**, **ESI†**), both of them exhibited greatly enhanced electrocatalytic activities for methanol electro-oxidation. This demonstrated that the shapes of the Pt-Au alloy nanocrystals have a profound effect on the catalytic activities. Furthermore, compared with Pt-Au alloy octahedra, the higher activity of Pt-Au alloy truncated trisoctahedra may be ascribed to their special surface structure with more ridges and high-energy concave edges. In addition, the chronoamperometry (CA) curve for the Pt-Au alloy truncated trisoctahedra exhibited a slower current attenuation with much high retention of current after 1000 s compared to other catalysts (**Fig. 6**b), revealing that the truncated trisoctahedral Pt-Au alloy nanocrystals could promote catalytic stability as well as activity in the electro-oxidation of methanol. In addition, the peak current ratio of the forward (I_f) to backward (I_b) scans reflects CO-poisoning tolerance, the larger the I_f/I_b ratio, the better the CO removal activity of the catalyst.[25] A slight increase of I_f/I_b ratio for truncated trisoctahedral Pt-Au alloy nanocrystals, compared to that of Pt black (**Table S2**, **ESI†**), indicated a better CO-poisoning tolerance. However, octahedral Pt-Au alloy nanocrystals, although it exhibited a higher I_f than that of Pt black, displayed a lower I_f/I_b ratio than that of Pt black, indicating that octahedral Pt-Au alloy nanocrystals reduced CO-poisoning tolerance.

In conclusions, uniform and well-defined truncated trisoctahedral or octahedral Pt-Au alloy nanostructures were successfully synthesized by reducing $H_2PtCl_6/HAuCl_4$ mixture in TEG under microwave irradiation for 140 s. The key to the success of morphology control for both types of bimetallic alloy nanostructures relies on $H_2PtCl_6/HAuCl_4$ molar ratio, the presence of KI, and co-reduction under microwave irradiation. The morphologies of Pt-Au alloy nanostructures can be well controlled by adjusting the molar ratio of $H_2PtCl_6/HAuCl_4$ precursors. The formation of Pt-Au alloy state was dependent upon the growth kinetics control which was manipulated by the use of KI. Furthermore, microwave irradiation facilitated the co-reduction of Pt(IV) and Au(III) species, in favour of the formation of Pt-Au alloy nanocrystals. Accordingly, the process provided a facile and efficient method for the controlled synthesis of bimetallic alloy nanocrystals with unique morphologies as well as different compositions. The as-prepared truncated trisoctahedral and octahedral Pt-Au alloy nanocrystals exhibited efficient electrocatalytic activities towards methanol oxidation.

Acknowledgements

This work was supported by the National Nature Science Foundation of China (Grant No. 21273289).

Notes and references

[a] *Key Laboratory of Catalysis and Material Science of the State Ethnic Affairs Commission & Ministry of Education, Hubei Province, College of Chemistry and Materials Science, South-Central University for Nationalities, Wuhan 430074, P. R. China. Fax: +86-27-67842752; Tel: +86-27-67843521; E-mail: huangt208@163.com.*

[b] *Institute of Chemistry, Chinese Academy of Science, Beijing, 100080, P. R. China.*

† Electronic Supplementary Information (ESI) available: Experimental details; SEM, TEM and HAADT-STEM images, UV-vis absorbance spectra, XRD. See DOI: 10.1039/b000000x/

1 *(a)* P. -P. Fang, A. Jutand, Z. -Q. Tian, C. Amatore, *Angew. Chem., Int. Ed*., 2011, **50**, 12184; *(b)* F. Wang, C. Li, L. -D. Sun, H. Wu, T. Ming, J. Wang, J. C. Yu, C. -H. Yan, *J. Am. Chem. Soc*., 2011, **133**, 1106; *(c)* Y. Ma, W. Li, E. C. Cho, Z. Li, T. Yu, J. Zeng, Z. Xie, Y. Xia, *ACS Nano*, 2010, **4**, 6725; *(d)* K. Zhang, Y. Xiang, X. Wu, L. Feng, W. He, J. Liu, W. Zhou, S. Xie, *Langmuir*, 2008, **25**, 1162; *(e)* J. Huang, Y. Zhu, M. Lin, Q. Wang, L. Zhao, Y. Yang, K. X. Yao, Y. Han, *J. Am. Chem. Soc*., 2013, **135**, 8552; *(f)* H. Liu and Q. Yang, *J. Mater. Chem*., 2011, **21**, 11961.

2 *(a)* Y. Yamauchi, A. Tonegawa, M. Komatsu, H. Wang, L. Wang, Y. Nemoto, N. Suzuki, and K. Kuroda, *J. Am. Chem. Soc.*, 2012, **134**, 5100; *(b)* F. Tao, M. E. Grass, Y. Zhang, D. R. Butcher, J. R. Renzas, Z. Liu, J. Y. Chung, B. S. Mun, M. Salmeron and G. A. Somorjai, *Science*, 2008, **322**, 932; *(c)* G. Chen, Y. Li, D. Wang, L. Zheng, G. You, C. J. Zhong, L. Yang, F. Cai, J. Cai, B. H. Chen, *J. Power Sources*, 2011, **196**, 8323; *(d)* C. Cui, L. Gan, H. –H. Li, S. –H. Yu, M. Heggen, and P. Strasser, *Nano Lett*., 2012, **12**, 5885; *(e)* Y. J. Deng, N. Tian, Z. Y. Zhou, R. Huang, Z. L. Liu, J. Xiao and S. G. Sun, *Chem. Sci*., 2012, **3**, 1157.

3 *(a)* S. Xie, N. Lu, Z. Xie, J. Wang, M. J. Kim, Y. Xia, *Angew. Chem., Int. Ed*., 2012, **51**, 10266; *(b)* J. Zeng, C. Zhu, J. Tao, M. Jin, H. Zhang, Z. Y. Li, Y. Zhu and Y. Xia, *Angew. Chem., Int. Ed*., 2012, **51**, 2354; *(c)* F.-R. Fan, D.-Y. Liu, Y.-F. Wu, S. Duan, Z.-X. Xie, Z.-Y. Jiang and Z.-Q. Tian, *J. Am. Chem. Soc*., 2008, **130**, 6949; *(d)* B. Lim, M. Jiang, P. H. C. Camargo, E. C. Cho, J. Tao, X. Lu and Y. Xia, *Science*, 2009, **324**, 1302; *(e)* Z. Peng and H. Yang, *J. Am. Chem. Soc*., 2009, **131**, 7542; *(f)* S. E. Habas, H. Lee, V. Radmilovic, G. A. Somorjai and P. Yang, *Nat. Mater*., 2007, **6**, 692.

4 *(a)* Y. W. Lee,M. Kim, Z. H. Kim and S.W. Han, *J. Am. Chem. Soc*., 2009, **131**, 17036; *(b)* J. W. Hong, Y. W. Lee, M. Kim, S. W. Kang and S. W. Han, *Chem. Commun*., 2011, **47**, 2553; *(c)* W. He, X. Wu, J. Liu, X. Hu, K. Zhang, S. Hou, W. Zhou and S. Xie, *Chem. Mater*., 2010, **22**, 2988; *(d)* G. Fu, L. Ding, Y. Chen, J. Lin, Y. Tang and T. Lu, *CrystEngComm*, 2014, **16**, 1606; *(e)* S. Garcia, R. M. Anderson, H. Celio, N. Dahal, A. Dolocan, J. Zhou, S. M. Humphrey, *Chem. Commun*., 2013, **49**, 4241..

5 *(a)* X. Huang, H. Zhang, C. Guo, Z. Zhou, N. Zheng, *Angew. Chem., Int. Ed*., 2009, **48**, 4808; *(b)* H. Zhang, M. Jin, J. Wang, W. Li, P. H. C. Camargo, M. J. Kim, D. Yang, Z. Xie, Y. Xia, *J. Am. Chem. Soc*., 2011, **133**, 6078; *(c)* J. W. Hong, S.W. Kang, B. S. Choi, D. Kim, S. B. Lee, S.W. Han, *ACS Nano*, 2012, **6**, 2410; *(d)* M. A. Mahmoud, M. A. El-Sayed, *Langmuir*, 2012, **28**, 4051; *(e)* H. Zhang, M. Jin, H. Liu, J. Wang, M. J. Kim, D. Yang, Z. Xie, J. Liu, Y. Xia, *ACS Nano*, 2011, **5**, 8212; *(f)* X. Hong, D. Wang, S. Cai, H. Rong, Y. Li, *J. Am. Chem. Soc*., 2012, **134**, 18165; *(g)* E. Gonzalez, J. Arbiol, V. F. Puntes, *Science*, 2011, **334**, 1377.; *(h)* M. Liu, Y. Zheng, S. Xie, N. Li, N. Lu, J. Wang, M. J. Kim, L. Guo, and Y. Xia, *Phys. Chem. Chem. Phys*., 2013, **15**, 11822.

6 *(a)* X. M. Lu, L. Au, J. McLellan, Z. Y. Li, M. Marquez, Y. N. Xia, *Nano Lett*., 2007, **7**, 1764; *(b)* M. McEachran, D. Keogh, B. Pietrobon, N. Cathcart, I. Gourevich, N. Coombs, V. Kitaev, *J. Am. Chem. Soc*., 2011, **133**, 8066; *(c)* H. J. Fan, U. Gçsele, M. Zacharias, *Small*, 2007, **3**, 1660; *(d)* W. Wang, M. Dahl, Y. Yin, *Chem. Mater*., 2013, **25**, 1179.

7 *(a)* J. Zhang, H. Yang, J. Fang and S. Zou, *Nano Lett*., 2010, **10**, 638; *(b)* J. Wu, J. Zhang, Z. Peng, S. Yang, F. T. Wagner and H. Yang, *J. Am. Chem. Soc*., 2010, **132**, 4984.

8 Y. Kim, J. W. Hong, Y. W. Lee, M. Kim, D. Kim, W. S. Yun, S. W. Han, *Angew. Chem., Int. Ed.*, 2010, **49**, 10197.

9 *(a)* E. K. Park, J. K. Lee, Y. S. Kim, G. P. Kim, S. H. Baeck, *J. Phys. Chem. Solids*, 2008, **69**, 1284; *(b)* J. Luo, M. M. Maye, V. Petkov, N. N. Kariuki, L. Wang, P. Njoki, D. Mott, Y. Lin, C. Zhong, *J. Chem. Mater*., 2005, **17**, 3086.

10 10 H. Li, H. Wu, Y. Zhai, X. Xu and Y. Jin, *ACS Catal.*, 2013, **3**, 2045.

11 *(a)* Y. Lee, J. Kim, D. S. Yun, Y. S. Nam, Y. Shao-Horn, *Energy Environ. Sci.*, 2012, **5**, 8328; *(b)* Y. Tan, J. Fan, G. Chen, N. Zheng and Q. Xie, *Chem. Commun*., 2011, **47**, 11624.

12 *(a)* S. Jung, L. Liu, K. L. Shuford and S. Park, *J. Phys. Chem. C*, 2013, **117**, 3141; *(b)* J. Liu, X. Hu, S. Hou, T. Wen, W. Liu, X. Zhu and X. Wu, *Chem. Commun.*, 2011, **47**, 10981; *(c)* S. Wang, N. Kristian, S. Jiang, X. Wang, *Electrochem. Commun*., 2008, **10**, 961; *(d)* L. Feng, X. Wu, L. Ren, Y. Xiang, W. He, K. Zhang, W. Zhou, and S. Xie, *Chem. Eur. J*., 2008, **14**, 9764.

20 13 J. Qu, H. Liu, F. Ye, W. Hu and J. Yang, *Int. J. Hydrogen Energy*, 2012, **37**, 13191.

14 C. Wang, W. Tian, Y. Ding, Y. Q. Ma, Z. L. Wang, N. M. Markovic, V. R. Stamenkovic, H. Daimon and S. Sun, *J. Am. Chem. Soc*., 2010, **132**, 6524.

25 15 X. Wu, L. Tan, D. Chen, X. Meng, and F. Tang, *Chem. Commun*., 2014, **50**, 539.

16 J. Wang, D. F. Thomas, A. Chen, *Chem. Commun*., 2008, **40**, 5010.

17 *(a)* S. Zhang, Y. Shao, H. G. Liao, J. Liu, I. A. Aksay, G. Yin and Y. Lin, *Chem. Mater*., 2011, **23**, 1079; *(b)* M. Schrinner, S. Proch, Y. Mei, R. Kempe, N. Miyajima and M. Ballauff, *Adv. Mater.*, 2008, **20**, 1928.

18 *(a)* P. Hernandez-Fernandez, S. Rojas, P. Ocon, J. L. Gomez de la Fuente, J. San Fabian, J. Sanza, M. A. Pena, F. J. García-García, P. Terreros, J. L. G. Fierro, *J. Phys. Chem. C*, 2007, **111**, 2913; *(b)* H. Ataee-Esfahani, L. Wang, Y. Yamauchi, *Chem. Commun*,. 2010, **46**, 3684; *(c)* H. Ataee-Esfahani, L. Wang, Y. Nemoto, Y. Yamauchi, *Chem. Mater*., 2010, **22**, 6310; *(d)* L. Wang, Y. Yamauchi, *Chem. Mater*., 2011, **23**, 2457.

19 *(a)* Y. Liu, Y. Wang, J. Zhang, S. Shi, P. Feng, T. Wang, *Catal. Commun*., 2009, **10**, 1244; *(b)* D. Seo, J, C. Park, H. Song, *J. Am. Chem. Soc*., 2006, **128**,14863; *(c)* C. Li, K. L. Shuford, Q.-H. Park,W. Cai, Y. Li, E. J. Lee, S. O. Cho, *Angew. Chem. Int. Ed*., 2007, **46**, 3264; *(d)* D. Y. Kim, W. Li, Y. Ma, T. Yu, Z.-Y. Li, O O. Park, Y. Xia, *Chem. Eur. J*., 2011, **17**, 4759.

20 C. D. Wagner, W. M. Riggs, L. E. Davis, J. F. Moulder, B. E. Muilenberg. *Handbook of X-ray Photoelectron Spectroscopy*, Perkin-Elmer, Physical Electronics Division, Eden Prairie, 1979.

50 21 L. Dai, Q. Chi, Y. Zhao, H. Liu, Z. Zhou, J. Li, T. Huang, *Mat er. Res. Bull*., 2014, **49**, 413.

22 B. L. Hayes, *Aldrichimica ACTA*, 2004, **37**, 66.

23 *(a)* T. Yu, D. Y. Kim, H. Zhang, Y. Xia, *Angew. Chem., Int. Ed*., 2011, **50**, 2773; *(b)* Y. J. Xiong, H. G. Cai, B. J. Wiley, J. G. Wang, M. J. Kim, Y. N. Xia, *J. Am. Chem. Soc*., 2007, **129**, 3665; *(c)* X. Huang, N. Zheng, *J. Am. Chem. Soc*., 2009, **131**, 4602; *(d)* S. E. Lohse, N. D. Burrows, L. S.carabelli, L. M. Liz-Marzan, C. J. Murphy, *Chem. Mater*., 2014, **26**, 34.

24 J. S. DuChene, W. Niu, J. M. Abendroth, Q. Sun, W. Zhao, F. Huo, and W. D. Wei, *Chem. Mater*., 2013, **25**, 1392.

25 *(a)* S. Zhang, S Guo, H. Zhu, D. Su, S. Sun, *J. Am. Chem. Soc*., 2012, **134**, 5060; *(b)* X. Sun, D. Li, Y. Ding, W. Zhu, S. Guo, Z. L. Wang, S. Sun, *J. Am. Chem. Soc*., 2014, **136**, 5745; *(c)* S. Sharma, A. Ganguly, P. Papakonstantinou, X. Miao, M. Li, J. L. Hutchison, M Delichatsios,. S. J. Ukleja, *J. Phys. Chem. C***,** 2010, **114**, 19459.